J Supercond Nov Magn (2015) 28:1–8
DOI 10.1007/s10948-014-2842-3

REVIEW PAPER

Evidence of Development of New Spin Orders Benefiting to Enhance Magnetic Properties in Co^{2+}-Doped Delafossite-Type Oxide $CuCrO_2$

T. Elkhouni · M. Amami · P. Strobel · A. Ben Salah

Received: 23 January 2014 / Accepted: 11 March 2014 / Published online: 25 November 2014

Abstract This paper reports the effect of high-spin Co^{2+}-doped $CuCrO_2$ delafossite-type oxide on the structure and physical properties. X-ray diffraction and Raman spectroscopy show that the structure is maintained for all Co-doped samples for chromium. The incorporation of this element generates anisotropic microstrains in the structure. The temperature dependence of zero field-cooling magnetization was measured. All samples exhibit an AFM transition around 24 K. The high-spin state and the shift due to the exchange splitting of the conduction band suggest strong hybridization between carriers in the Cr 3d t_{2g} band and the t_{2g} states of the high-spin Co^{2+} to develop other spin orders benefiting to enhance magnetic susceptibility and support the evidence of new FM transition. The coupling between the magnetic order and ferroelectric order is also characterized.

Keywords Delafossite oxides · XRD · Magnetic properties · Raman spectroscopy · Dielectric permittivity

T. Elkhouni (✉) · M. Amami · A. Ben Salah
Laboratoire des Sciences de Matériaux et d'environnement, Faculté des Sciences de Sfax, BP 763, 3038, Sfax, Tunisia
e-mail: elkhouni@yahoo.fr

P. Strobel
Institut Néel, CNRS, Université Joseph Fourier, B.P. 166, 38042, Grenoble Cedex 9, France

M. Amami
Unité de Recherche de Chimie des Matériaux, ISSBAT, Université Tunis El Manar, 9, Avenue Dr. Zouhaier Safi, 1006 Tunis, Tunisia

T. Elkhouni
Laboratoire de Valorisation des Matériaux Utiles, Centre National des Recherches en Sciences des Matériaux, Borj Cedria, BP 174, 1164, Hammam-Chatt, Tunis, Tunisia

1 Introduction

The delafossite oxide $CuMO_2$ (M = trivalent cation or mixture of trivalent and bivalent cations) [1, 2] is one of a number of systems possessing an antiferromagnetic triangular sublattice. $CuMO_2$ has a layered structure with a space group of R-3m, which is viewed as the alternate stacking of edge-shared MO_6 octahedral (MO_2) layers and Cu layers. Remarkably, all these structural families are based on CdI_2-type layers containing first-row transition metals and oxygen. In the delafossite crystal structure, MO_2 layers of edge-sharing MO_6 octahedra alternate along the c axis with layers of monovalent Cu^+ cations with dumbbell O–Cu–O coordination. Interesting thermoelectric performances have been reported in delafossite-type oxides.

The magnetic properties of these layered compounds have attracted much attention, since the geometrical frustration in the magnetic triangular sublattice at the M sites causes intriguing properties, such as field-induced multistep magnetization change [3, 4] and multiferroics [5]. $CuCrO_2$ is reported to exhibit both antiferromagnetic [6] and ferroelectric [7] behaviors below its Néel temperature, $T_N = 25$ K. Delafossites have been particularly investigated because of the diversity of their physical properties.

Another reason is the discovery of spin-driven multiferroicity in the layered delafossite compound $CuFeO_2$ [8], which leads us to study the parent oxide $CuCrO_2$, to which only a few studies had been dedicated. The magnetic properties of $CuCrO_2$ were investigated by Doumerc et al. [9] in the two-dimensional (2D) Heisenberg framework. In their pioneer work on the investigation by neutron powder diffraction of the magnetic structure of $CuCrO_2$, Kadowaki et al. [10] proposed several possible magnetic models and reported strong magnetic disorder in the stacking c direction. Very recently, $CuCrO_2$ was reported to

show ferroelectric polarization upon spin ordering, [11] suggesting a strong coupling between ferroelectricity and the assumed 120° spiral structure. Several points remained unclear however; because of the lack of low-temperature structural data, it was not known whether $CuCrO_2$ exhibits a structural phase transition similar to the one observed in $CuFeO_2$ and which could explain the observed three-dimensional (3D) magnetic ordering in a triangular lattice, whose ground state should otherwise stay degenerated.

In this work, we focus on the effect of magnetic Co^{2+} substitution on the structural, magnetic, and dielectric properties of $CuCrO_2$ (system $CuCr_{1-x}Co_xO_2$).

2 Experimental

Polycrystalline samples of Co^{2+}-doped $CuCrO_2$ for different compositions around 6 % were prepared using the standard solid-state reaction. Stoichiometric mixtures (0.5 g) of Cu_2O, Cr_2O_3, and CoO were ground and pressed in pellets. The samples were fired repeatedly in air at 1,150 °C for 12 h in alumina crucibles with intermediate regrinding and pelletizing. X-ray powder diffraction patterns of the products were collected with a PANalytical diffractometer equipped with a CuK_a source ($K_{\alpha 1}$ and $K_{\alpha 2}$) in the 2θ range from 10° to 90° at room temperature.

Strain and size components were extracted from line widths using the Williamson–Hall (WH) analysis [12]. This method uses the fact that the crystallite size and strain contributions to the line widths vary differently with the diffraction angle. The equation used is

$$L \cdot \cos\theta = \frac{\lambda}{D} + k\varepsilon \sin\theta$$

where L is the integral width; λ the wavelength; D the size of coherent diffraction domains, which is a near-unity constant; and ε th microstrain term. As a result, a plot of $(L{\cdot}\cos\theta)$ as a function of $(\sin\theta)$ yields D from the constant term and ε from the slope.

Raman spectra were recorded at room temperature with the 514.5-nm excitation from a Spectra Physics krypton ion laser. The compounds were studied with a low laser power (102 mW). One scanning of 60 s has been used for each sample. No damage of the material by the laser has been observed. The beam was focused onto the samples using the macroscopic configuration of the apparatus.

Magnetization measurements vs. temperature were carried out in a Quantum Design superconducting quantum interference device (SQUID) magnetometer in the range 4–300 K.

The typical field used for temperature dependence measurements was 0.1 T. Specific heat was measured in zero magnetic fields by a relaxation method. Dielectric data were collected using an impedance analyzer.

3 Results and Discussion

3.1 Structural Characterization

Figure 1 shows the XRD patternse of Co^{2+}-substituted delafossite $CuCrO_2$, in which all the peaks are indexed as the delafossite structure (space group *R-3m*), except for $x = 0.06$, where the same picture shows a small amount of impurities, around 2 % of cobalt oxides and spinel. $CuCr_2O_4$ was also detected.

The reflections of substituted samples are shifted to lower values of 2θ, indicating a lattice parameter increase with substitution. The lattice parameters a and c of the samples are given in Fig. 2.

Since Co^{2+} and Cr^{3+} do not have the same oxidation state, Co^{2+} substitution for Cr^{3+} is expected to introduce mainly atomic disorder in the Cr network. In addition, this disorder is probably related to the introduction of strains in the lattice, since Co^{2+} is a much larger cation than Cr^{3+} [13]. These results are in good agreement with those reported by Okuda et al. [14]. This increase in ionic radius ($r_{Cr3+} = 0.61$ Å, $r_{Co2+} = 0.78$ Å) causes the distortion of the network and the increase in lattice parameters. It seems that O–Cu–O bond lengths along the c axis are quite almost not affected by the chromium to cobalt substitution, whereas a parameter increases proportionally to the edge of the MO_6 octahedral when x increases. This anisotropy induces a constant increase of the distortion of the MO_6

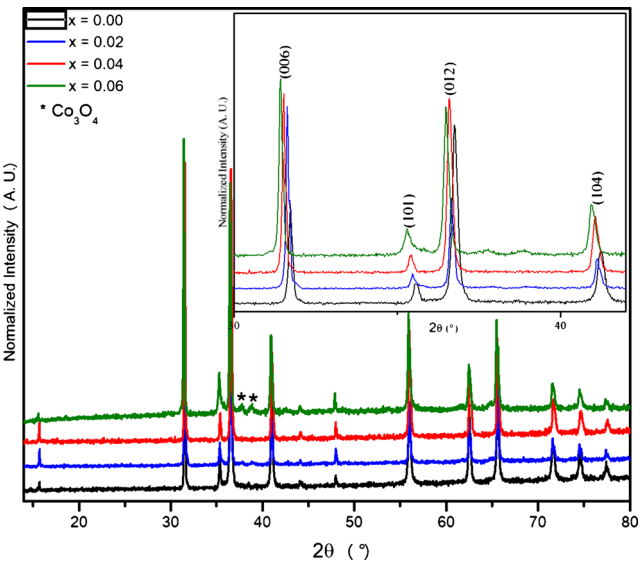

Fig. 1 XRD patterns of $CuCr_{1-x}Co_xO_2 (0 < x < 0.06)$ samples with a rhombohedral delafossite structure

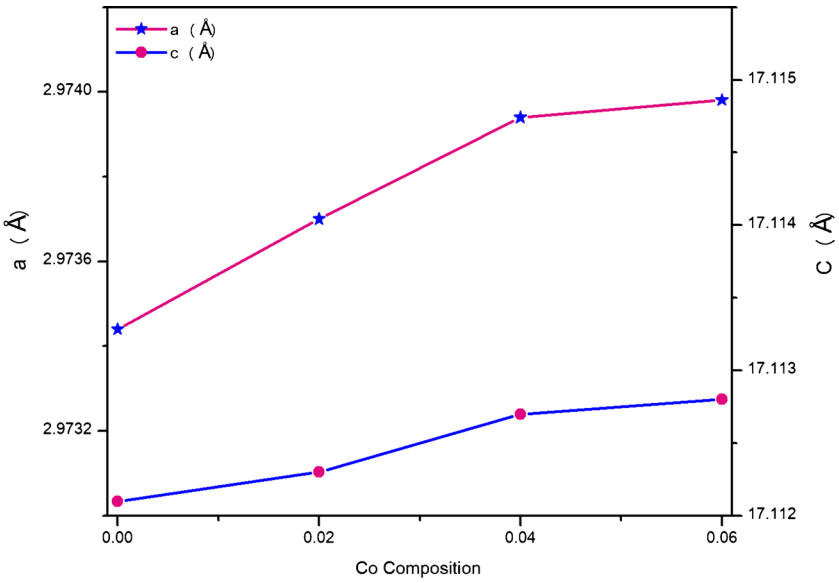

Fig. 2 Variation of refined unit cell parameters a and c as a function of x in $CuCr_{1-x}Co_xO_2$ $(0 \leq x \leq 0.06)$

octahedra from chromium to cobalt, which can be correlated to the covalence of the metal-to-oxygen bond [15].

The structure of $CuCr_{1-x}Co_xO_2(0 \leq x \leq 0.06)$ closely is delafossite. It consists of close-packed oxygen sheets in which the octahedral sites are occupied by Cr^{3+}/Co^{2+} ions. The $(Cr/Co)O_6$ octahedra share six edges to form infinite $\{(Cr/Co)O_2\}_\infty$ layers connected to each other by Cu^+ linearly bonded to two oxygen to form $(O-Cu-O)^{3-}$ "dumbbell" parallel to the c axis. Each Cu^+ is surrounded by six coppers hexagonally arranged in the (a, b) plane. Strain generated by the Co substitution was determined from the Williamson–Hall relationship. Plots of $(L{\cdot}\cos\theta)$ as a function of $(\sin\theta)$ are given in Fig. 3. They show a remarkable difference in angular dependence of the line width for different families of interreticular planes: the $h0l$ planes

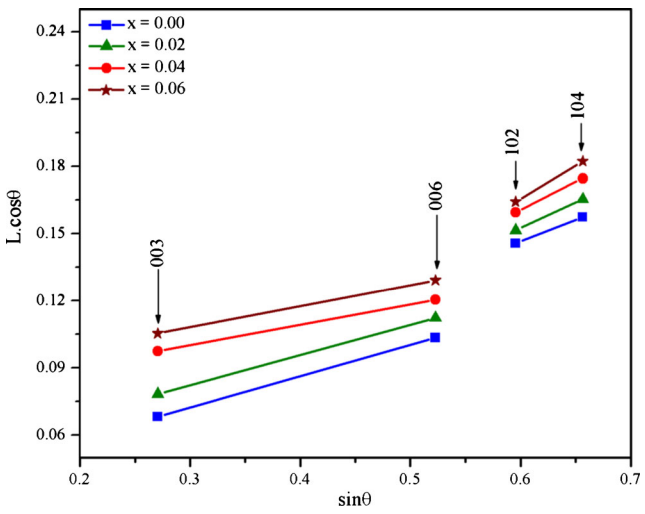

Fig. 3 Williamson–Hall plot of integral line width L

yield an important contribution of microstrains (high slope), while this effect is almost negligible in 00l planes. This shows that this material behaves rather anisotropically and that strains affect mostly bonding in the basal ab planes.

3.2 Raman Spectroscopic

The delafossite structure belongs to point group C_{3v} and space group $R\text{-}3m$. The four atoms in the primitive cell of the rhombohedral $R\text{-}3m$ structure give rise to 12 optical phonon modes in the zone center ($k{\sim}0$): three acoustic and nine optical modes. The latter are $\Delta_{opt.R3c} = A_{1g} + E_g + 3A_{2u} + 3E_u$. Among these, the two phonon modes with A_{1g} and E_g symmetry are Raman active. The former arise from the Cu–O bond vibration along the c axis, whereas the doubly degenerate E modes describe the vibrations along the a axis. The existence of an inversion center in the delafossite structure could classify the normal modes in terms of their parity. The odd modes, denoted with the "u" subscript, are the acoustic modes $(A_{2u} + E_u)$ which are IR active. Since there is only one mode of each symmetry, the exact eigenvector is determined without requiring any lattice dynamical model. Pellicer-Porres et al. [16] have discussed the phonon dispersion at the zone center for $CuGaO_2$ delafossite. They proposed that the inversion center is lost along the direction of $\Gamma(T)$ direction and the symmetry is reduced from D_{3d} to C_{3v}. According to compatibility relations, A_{1g} and A_{2u} on one hand and E_g and E_u modes on the other transform to A_1 and E modes, respectively.

To further study the doping effect on the structure by the replacement of Cr^{3+} with Co^{2+} ions, Raman spectroscopy was performed with 514.5-nm excitation light. Figure 4 shows the Raman spectra of $CuCr_{1-x}Co_xO_2$ for different

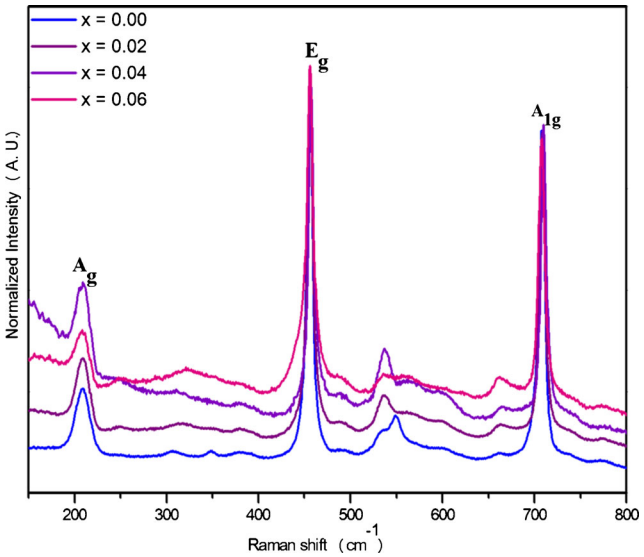

Fig. 4 Raman spectroscopy of $CuCr_{1-x}Co_xO_2$ ($0 \leq x \leq 0.06$) bulk samples at room temperature

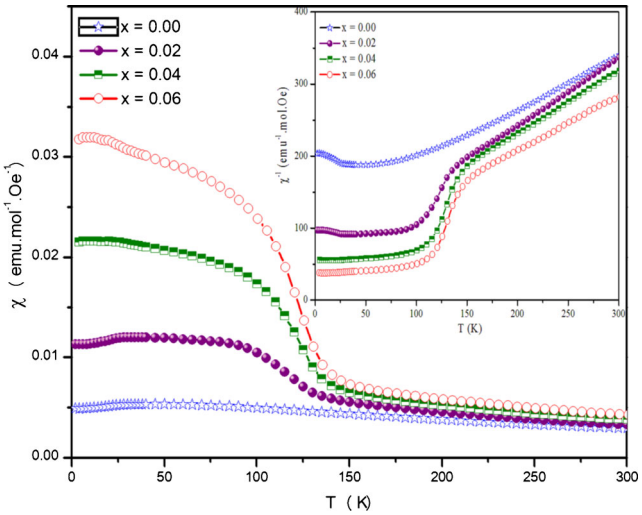

Fig. 5 The temperature dependence of zero field-cooling susceptibility (χ–T curve) of $CuCr_{1-x}Co_xO_2$ ($0 \leq x \leq 0.06$) samples. *Inset*: Temperature (T) dependence of the inverse susceptibility

cobalt contents. Three Raman peaks were observed for all samples around 453(A_g), 531(E_g), and 707 cm^{-1}(A_{1g}), which agree well with earlier studies on those compounds with delafossite structure [16, 17]. The A_{1g} mode corresponded to the (Cr/Co)–O stretching of $(Cr/Co)O_6$ octahedra and the E_g mode to the O–(Cr/Co)–O bending. This assignment was based on the fact that the movement of oxygen atoms attached to the central metal atom viz, (Cr/Co), was responsible for the observed Raman modes. Those results showed that Co substitution did not change the delafossite structure of the material. As shown in Fig. 4, Co-doped samples induce a slight increase in linewidth of the three active Raman modes A_g, A_{1g}, and E_g, indicating an increasing in (Cr/Co)–O bonding, which is consistent with the observed lattice increase along the different axes and the difference in ionic radius between Cr^{3+} and Co^{2+}.

3.3 Magnetic Properties

Figure 5 shows the temperature dependence of zero field-cooling susceptibilities (χ–T curve) of the $CuCr_{1-x}Co_xO_2$ ($0 \leq x \leq 0.06$) samples, where a 0.1-T magnetic field was applied. For the first distinguishing, it can be clearly seen that the magnetic susceptibility increases with the increases of the molar concentration in the all compounds. This increase of the magnetic susceptibilities for all samples in the temperature range 2–30 K may be due to interaction between Co^{2+} and Cr^{3+} spin systems. In all the curves of susceptibilities, an anomaly appears at 25 K owing to an antiferromagnetic (AFM) transition. The Néel transition (T_N) is almost consistent with the one previously reported [10]. They assume that the samples are not in a phase-separated state as composed of $CuCrO_2$ (T_N = 24 K) [10, 18]. At this temperature and above 130 K, all samples are in the paramagnetic state.

Abrupt increases in magnetization appear between 100 and 130 K shown in Fig. 4. It implies a FM transition which should be due to the FM interaction through the Co^{2+}–O–Cr^{3+} and in $CuCr_{1-x}Co_xO_2$($0 \leq x \leq 0.06$) exchange in the first time. All these changes in the χ–T curves in the two systems indicate a competition between AFM and FM interactions, and it also indicates that the DE interaction between the Co^{2+} and Cr^{3+} ions is very important.

Correlating the increases in lattice parameters a and c in $CuCr_{1-x}Co_xO_2$system with increase in magnetic susceptibility and the development of the new FM transition, the increases of the in-plane lattice parameter indicate that the valence state of Co ions was not Co^{3+} (*HS*) or Co^{3+} (*L·S*) according to the data of the ionic radius of sixfold coordinated Co and Cr (Co^{3+} (*HS*): 0.61 Å, Co^{3+} (*L·S*): 0.52 Å, and Cr^{3+}: 0.615 Å) [19] as well as lattice expansion. The lattice parameters a and c would increase if the valence state of the Co ions is 2+ in Co-doped $CuCrO_2$ semiconductors because the ionic radii of Co^{2+} are larger than that of Cr^{3+} (Co^{2+} (*HS*): 0.73 Å, and Co^{2+} (L·S): 0.65 Å) [19]. The development of the new FM transition proves that Co^{2+} is $H{\cdot}S$ ($S = 3/2$), because of its Co^{2+} $L{\cdot}S$ ($S = 1/2$); all samples do not develop a FM transition, and during the coupling spin between Co^{2+} $L{\cdot}S$ ($S = 1/2$) and Cr^{3+} ($S = 3/2$), the antiferromagnetic (AF) transition becomes broader and the magnetic susceptibility decreases with increasing of Co content. However, it would remain constant that Co ions is 2+ (*HS*) since the ionic radius of Co^{2+} ($H{\cdot}S$) is larger than that of Cr^{3+}, whereas the valence state of Co ions cannot be totally confirmed by the changes in the lattice parameters.

The exchange interaction was extensively studied in many works. Li et al. [20] proposed that the Mn^{3+}–O–Cr^{3+} exchange interaction in $CuCr_{1-x}Mn_xO_2$ system is superexchange (SE). Ohtsuki et al. [21] supposed that the magnetic interactions between Co^{2+} and Co^{2+} ions taking the high-spin configuration should develop weak ferromagnetic interactions; those interactions between Cr^{3+} and Cr^{3+} ions in the mother $CuCrO_2$ are antiferromagnetic [22]. The anisotropic magnetic interactions of the *A*-type structure and induced three-dimensional ferromagnetic interactions in $CuCoO_2$ compounds show a weak ferromagnetism, by introducing some metal transition in three valences in Co sites. Such a Cr doping on the Co site enhances the ferromagnetic interaction in these compounds.

On the other hand, Li et al. [20] reported that the Mn substitution in Cr sites of the mother compound $CuCrO_2$ induces disorder on the Cr sites and prevents the establishment of conducting paths along the Mn–O–Cr bonds. Conversely, the introduction of trivalent cations does not induce a strong ferromagnetism and the electronic transport is obviously hindered by these foreign cations on the Cr sites. This supposition explains the strong ferromagnetic transition in $CuCr_{1-x}Mn_xO_2$ which is induced by introducing mixed-valent manganese Mn^{3+}/Mn^{4+}, and they induce disorder on the Mn sites. These phenomena explain the variation of the amplitude transition ferromagnetic with the temperature. It is clearly seen that this FM transition in high-spin configuration of Co-doped $CuCrO_2$ in the temperature range around 130 K increases with increasing of Co content. All those results we obtained support the evidence of the FM transition in newly developed Co-doped $CuCrO_2$. The high-spin state and the shift due to the exchange splitting of the conduction band suggest strong hybridization between carriers in the Cr 3d t_{2g} band and the t_{2g} states of the high-spin Co^{2+}. These observations support the argument that the temperature of FM transition in high-spin Co^{2+}-doped $CuCrO_2$ is intrinsic. It is clearly seen that this FM transition around 130 K increases with Co content and might be attributed either to the Co^{2+}–O–Cr^{3+} exchange interaction (Co^{2+} *HS* ($S = 3/2$)) which help to tune the spin chirality and to develop other spin orders benefiting to enhance magnetic susceptibility.

In the paramagnetic states, χ^{-1}–T (inset of Fig. 5) obeys a Curie–Weiss form $\chi = C/(T + \Theta_{cw})$ where C and Θ_{cw} (≥ 0) are the Curie–Weiss constant and magnetic coupling parameter, respectively. Abrupt increases in magnetic susceptibility appear which explain the effect of Co-doped $CuCrO_2$.

The estimated C and Θ_{cw} are given in Table 1. Around T_N, an anomaly associated with a three-dimensional antiferromagnetic (AFM) order was observed up to well with previous by [23].

Table 1 Estimated Curie constant, Curie temperature, and effective magnetic moment from the high temperature of paramagnetic region for $CuCr_{1-x}Co_xO_2$ ($0 \leq x \leq 0.06$) compounds

Samples	C (emu·mol^{-1}·K)	θ (K)	$\mu_{eff(exp.)}$ (μ_B)
$CuCrO_2$	1.805 (7)	−260.02 (8)	3.800 (8)
$CuCr_{0.98}Co_{0.02}O_2$	1.877 (2)	−248.56 (6)	3.875 (2)
$CuCr_{0.96}Co_{0.04}O_2$	1.914 (3)	−234.83 (1)	3.913 (3)
$CuCr_{0.94}Co_{0.06}O_2$	2.119 (8)	−194.65 (4)	4.118 (1)

All data yield highly negative Θ_{cw} values, indicating dominant antiferromagnetic interactions. Therefore, the observed increase of $|\Theta|$ might be attributed to the effect of Co^{2+}, as the number of magnetic nearest neighbors should decrease as the Cr concentration is more and more accentuated.

An effective moment by formula unit can be extracted using the following formula:

$$\left(\mu_{eff}/\mu_B\right)^2 = 3k_BC/N \quad (1)$$

where k_B = Boltzmann constant, C = Curie constant, N = Avogadro's number, and μ_B = Bohr magneton. In the spin-only picture usually followed for localized spins of 3d ions, μ_{eff} is given by

$$\mu_{eff} = g\left[S\left(S+1\right)\right]^{1/2}\mu_B \quad (2)$$

where $g \approx 2.0$. The experimental values of μ_{eff} are all slightly lower than the theoretical spin-only value for Cr^{3+} ($\mu_{eff}/\mu_B = \sqrt{15} = 3.87$). These results are consistent with the behavior commonly observed for 3d cations, where the incomplete quenching of orbital moments yields lower values of μ_{eff}. The effective moments lie between 3.8 and 4.11 μ_B, which are closely constant. These results lead to the consideration that Co ions in the delafossite structure are mainly in bivalent high-spin state ($S = 3/2$) which explains the constancy of the effective moments in substitution of Cr^{3+} ($S = 3/2$) by Co^{2+} *HS* ($S = 3/2$), contrary to those in $CuCoO_2$ [24] and $AgCoO_2$ [25].

The interaction of the Cr and Co cations with each other through Cr–O–Co linkages of approximately 180° is expected to be the dominant consideration, and this would be antiferromagnetic in nature. Recently, evidence of room temperature ferromagnetism in Co-doped transparent $CuAlO_2$ semiconductor was reported. Specially, the coercivity (Hc) and saturation magnetization are significantly enhanced with Co composition [26]. To further reveal this point, we present the measured χ–H hysteresis at $T = 4$ K for $CuCr_{1-x}Co_xO_2$ ($x = 0.00$ and 0.06) as shown in Fig. 6. While no loop for $CuCrO_2$ is shown, a remarkable loop for $CuCr_{1-x}Co_xO_2$ ($x = 0.06$) is observed, giving rise to a coercivity of 5,000 Oe and remnant magnetization of ~4.75 E^{-4} emu·mol^{-1}, although no magnetization

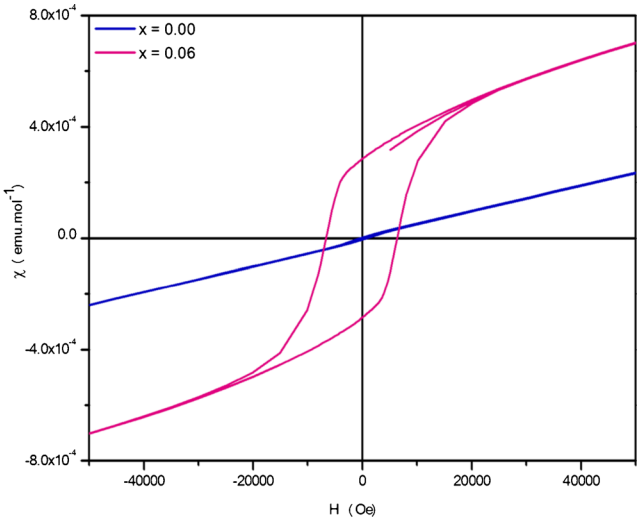

Fig. 6 χ–H relationship of $CuCr_{1-x}Co_xO_2$ ($x = 0.00$ and 0.06) at 4 K. Clear hysteresis loops are observed, confirming a FM order induced by high-spin Co^{2+} doping in $CuCrO_2$ semiconductors

saturation is obtained, probably due to the spin-glasslike essence. Therefore, the substantial ferromagnetic component in the magnetism of $CuCr_{1-x}Co_xO_2$ is revealed. The observed magnetic behavior for $CuCr_{1-x}Co_xO_2$ is probably due to the disorder of Cr and Co in octahedral sites resulting in short-range Cr–O–Cr and Cr–O–Co interactions between which could give rise to antiferromagnetism coupled with short-range weak ferromagnetism. Thus, the observed ferromagnetism is essentially intrinsic to some extent.

Figure 7 shows the temperature dependence of specific heat (C) for $CuCr_{1-x}Co_xO_2$ ($x = 0.00$ and 0.06). For both

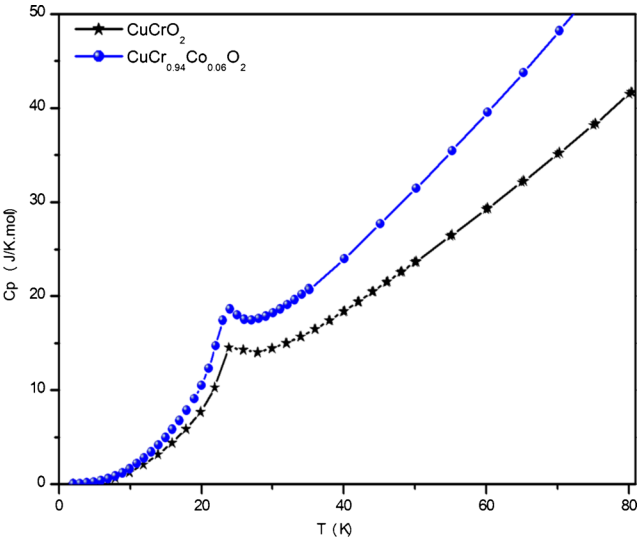

Fig. 7 Temperature dependence of specific heat (C) of $CuCr_{1-x}Co_xO_2$ for $x = 0$ and $x = 0.06$

compounds, the electric contribution to specific heat is negligible at low temperatures [27]. This figure clearly shows that the specific heat peak at T_N becomes broader and that the peak temperature (T_{peak}) increases with increase in x. Such x dependence of C is apparently correlated with magnetization (M) [3]. Corresponding to the AFM transition, a sharp peak is observed at about 24 K. In addition to the sharp peak, a broad shoulder is observed around 24 K. Such a broad C (T) peak profile is often observed in frustrated kagome [28] or triangular [29] AFM lattices and indicates high degeneracy due to magnetic frustration which was also observed for all $CuCr_{1-x}Mg_xO_2$ compounds [30].

3.4 Dielectric Properties

Figure 8a, b—combining also susceptibility curves and dielectric permittivity—reveals a clear relationship between the temperature of the dielectric anomaly and the T_N. The strength of the dielectric anomaly increases by increasing the cobalt content in $CuCrO_2$.

The anomaly in dielectric permittivity associated with the noncollinear antiferromagnetic phase has been reported previously for $CuCrO_2$ and Al-doped $CuCrO_2$. Dielectric permittivity anomaly was observed around magnetic transition

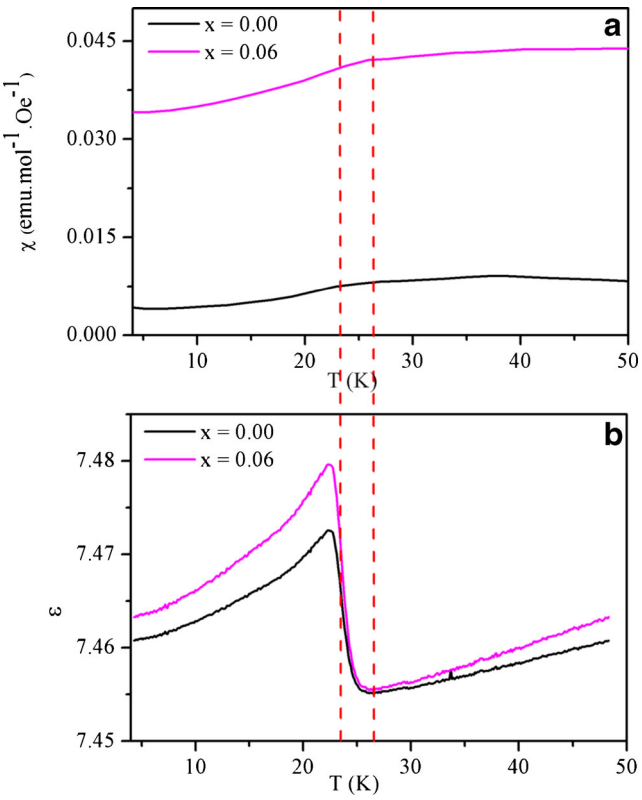

Fig. 8 Temperature dependence of **a** susceptibility and **b** dielectric constant ε for $CuCrO_2$ and $CuCr_{0.94}Co_{0.06}O_2$

temperature, indicating magnetoelectric coupling in these samples. The increase of the dielectric permittivity at Neel temperature T_N is related to thermally induced enhancement of the hopping conduction [31–33], which is caused by oxygen ion vacancies causing stabilization of the Cr–O couple–oxygen vacancy interaction.

The susceptibility (χ) curve exhibits a well-defined anomaly with a maximum near 24 K which is also correlated with a dielectric anomaly (Fig. 8b). The broad dielectric anomaly starting at about 24 K with a maximum near 23 K (Fig. 8a) can therefore be associated with the formation of antiferromagnetic phase, from paramagnetic to antiferromagnetic structure. Co doping affects both dielectric permittivity and magnetization curves (Fig. 8a, b). In particular, for $CuCr_{1-x}Co_xO_2$, $x = 0.04$, it was observed that the anomaly is shoulder like and the Neel temperature is shifted towards lower temperature region ($T_N = 24$ K; Fig. 8b). This anomaly seems also to be an indication of AFM ordering [34, 35]. At almost the same temperature, a clear peak in the dielectric permittivity is induced by Co^{2+} substitution for Cr^{3+} (Fig. 8a). Further, doping effect could be more evidenced by measuring polarization, which was not available for us during this study. These anomalies are clear indications of the ME coupling, and the underlying physics is straightforward by considering the fact that the AFM order with the proper spin chirality can be further stabilized by the established ferroelectric order via their coupling.

4 Conclusion

We have prepared polycrystalline $CuCr_{1-x}Co_xO_2$ ($0 \leq x \leq 0.06$) samples by solid-state reaction. In the present work, we reported the effect of high-spin Co^{2+}-doped $CuCrO_2$ on structural, physical, and spectroscopic properties. The Co incorporation in the delafossite structure generates microstrains showing an anisotropical behavior. The increased strain is likely due to some absence of uniformity of the distribution for incorporated oxygen. Raman spectroscopy showed that Co substitution did not change the delafossite structure of the material. However, the relative intensity of Raman peaks changes rapidly with the content and the peak position also shifts towards shorter wavenumbers, indicating the increase of the lattice distortion with the substitution. It has been revealed that the high-spin Co^{2+}-doping $CuCrO_2$ accentuated the magnetic susceptibility. It is argued that the high-spin state of Co^{2+} doping destabilizes the antiferromagnetic order of Cr^{3+} ions, modulates the spin configuration, and suggests a strong hybridization between carriers in the Cr 3d t_{2g} band and the t_{2g} states of the high-spin Co^{2+} to develop other spin orders benefiting to enhance magnetic susceptibility and support the evidence of new FM transition. Clear hysteresis loops check that FM order exists at 4 K.

References

1. Elkhouni, T., Colin, C.V., Strobel, P., Ben Salah, A., Amami, M.: J. Supercond. Nov. Magn. **7**, 1807 (2012)
2. Elkhouni, T., Amami, M., Strobel, P., Ben Salah, A.: J. Supercond. Nov. Magn. **7**, 2256 (2013)
3. Okuda, T., Jufuku, N., Hidaka, S., Terada, N.: Phys. Rev. B **72**, 144403 (2005)
4. Terada, N., Nakamura, Y., Katsumata, K., Yamamoto, T., Staub, U., Kindo, K., Hagiwara, M., Tanaka, Y., Kikkawa, A., Toyama, H., Fuyuki, T., Kanmuri, R., Ishikawa, T., Kitamura, H.: Phys. Rev. B **74**(R), 180404 (2006)
5. Kimura, T., Lashley, J.C., Ramirez, A.P.: Phys. Rev. B **73**(R), 180404 (2006)
6. Attili, R.N., Uhrmacher, M., Lieb, K.P., Ziegeler, L., Mekata, M., Schwarzmann, E.: Phys. Rev. B **53**, 600 (1996)
7. Kumar, S., Singh, K., Miclau, M., Simon, C., Martin, C., Maignan, A.: J. Solid State Chem. **4596**, 00197–7 (2013)
8. Kimura, T., Lashley, J.C., Ramirez, A.P.: J. Phys. Rev. B **73**, 220401R (2006)
9. Doumerc, J.P., Wichainchai, A., Ammar, A., Pouchard, M., Hagenmuller, P.: J. Mater. Res. Bull. **21**, 45 (1986)
10. Kadowaki, H., Kikuchi, H., Ajiro, Y.: J. Phys.: Condens. Matter. **2**, 4485 (1990)
11. Seki, S., Onose, Y., Tokura, Y.: J. Phys. Rev. Lett. **101**, 067204 (2008)
12. Williamson, G.K., Hall, W.H.: Acta Metall. **1**, 22 (1953)
13. Shannon, R.D., Rogers, D.B., Prewitt, C.T.: Inorg. Chem. **10**, 713 (1971)
14. Okuda, T., Beppu, Y., Fujii, Y., Onoe, T., Terada, N., Miyasaka, S.: Phys. Rev. B **77**, 134423 (2008)
15. Doumerc, J.P., Ammar, A., Wichainchai, A., Pouchard, M., Hagenmuller, P.J.: Phys. Chem. Solids **48**, 37–43 (1987)
16. Pellicer-Poress, J., Martinez-Garcia, D., Segura, A., Rodrigez-hernandez, P., Munoz, A., Chervin, J.C.: Phys. Rev. B **74**, 18430 (2006)
17. Elkhouni, T., Amami, M., Hlil, E.K., Ben Salah, A.: J Supercond. Nov. Magn. **8**, 2182 (2013)
18. Okuda, T., Kishimoto, T., Uto, K., Hokazono, T., Onose, Y., Tokura, Y., Kajimoto, R., Matsuda, M.: J. Phys. Soc. Jpn. **78**, 013604 (2009)
19. Deisenhofer, J., Paraskevopoulos, M., Krug von Nidda, H.-A., Loidl, A.: J. Phys. Rev. B **66**, 054414 (2000)
20. Li, D., Fang, X., Dong, W., Deng, Z., Tao, R., Zhou, S., Wang, J., Wang, T., Zhao, Y., Zhu, X.: J. Phys. D: Appl. Phys. **42**, 055009 (2009)
21. Quilty, J.W., Shibata, A., Son, J.Y., Takubo, K., Mizokawa, T., Toyosaki, H., Fukumura, T., Kawasaki, M.: J. Phys. Rev. Lett. **96**, 027202 (2006)
22. Yang, Z., Ye, L., Xie, X.: J. Phys.: Condens. Matter. **12**, 2737–2747 (2000)
23. Amami, M., Colin, C.V., Strobel, P., Ben Salah, A.: J. Physica B **406**, 2182–2185 (2011)
24. Beekmana, M., Salvadorb, J., Shic, X., Nolasa, G.S., Yang, J.: J. All. Comp. **489**, 336 (2010)
25. Muguerra, H., Colin, C., Anne, M., Julien, M.-H., Strobel, P.: J. Sol. Stat. Chem. **181**, 2883 (2008)
26. Dong, C.J., Yu, W.X., Xu, M., Cao, J.J., Zhang, Y., Chuai, Y.H., Wang, Y.D.: J. All. Comp. **512**, 195 (2012)

27. Okuda, T., Beppu, Y., Fujii, Y., Onoe, T., Terada, N., Miyasaka, S.: Phys. Rev. B **77**, 134423 (2008)
28. Ramirez, A.P., Hessen, B., Winklemann, M.: Phys. Rev. Lett. **84**, 2957 (2000)
29. Nakatsuji, S., Nambu, Y., Tonomura, H., Sakai, O., Jonas, S., Broholm, C., Tsunetsugu, H., Qiu, Y., Maeno, Y.: Science **309**, 1697 (2005)
30. Okuda, T., Beppu, Y., Fujii, Y., Kishimoto, T., Uto, K., Onoe, T., Jufuku, N., Hidaka, S., Terada, N., Miyasaka, S.: J. Phys. Conf. Ser. **150**, 042157 (2009)
31. Huang, F., Lu, X., Lin, W., Wu, X., Kan, Y.: J. Appl. Phys. Lett. **89**, 242914 (2006)
32. Hiroshi, U., Risako, U., Hiroshi, F., Koda, S.: J. Appl. Phys. **100**, 014106 (2006)
33. Mishra, R.K., Pradhan, D.K., Choudhary, R.N.P., Banerjee, A.: J. Phys. Condens. Matter. **20**, 045218 (2008)
34. Luo, S., Li, L., Wang, K.F., Li, S.Z., Dong, X.W., Yan, Z.B., Liu, J.M.: Thin Solid Films **518**, e50 (2010)
35. Kimura, K., Nakamura, H., Ohgushi, K., Kimura, T.: Phys. Rev. B **78**, 140401(R) (2008)